International Journal of Bifurcation and Chaos, Vol. 11, No. 10 (2001) 2587–2605

RESONANCE STRUCTURE IN A WEAKLY DETUNED LASER WITH INJECTED SIGNAL

CATALINA MAYOL
Departament de Física, Universitat de les Illes Balears and Instituto Mediterráneo de Estudios Avanzados (IMEDEA, UIB-CSIC), E-07071 Palma de Mallorca, Spain

MARIO A. NATIELLO
Centre for Mathematical Sciences, Lund University, Box 118 S-22100 Lund, Sweden

MARTÍN G. ZIMMERMANN
Departamento de Física, FCEyN–Universidad de Buenos Aires, Pabellón I, Ciudad Universitaria, 1428 Buenos Aires, Argentina

Received October 5, 2000; Revised December 13, 2000

We describe the qualitative dynamics and bifurcation set for a laser with injected signal for small cavity detunings. The main organizing center is the Hopf-saddle-node bifurcation from where a secondary Hopf bifurcation of a periodic orbit originates. We show that the laser's stable cw solution existing for low injections, also suffers a secondary Hopf bifurcation. The resonance structure of both tori interact, and homoclinic orbits to the "off" state are found inside each Arnold tongue. The accumulation of all the above resonances towards the Hopf-saddle-node singularity points to the occurrence of a highly degenerate global bifurcation at the codimension-2 point.

1. Introduction

The control of a laser via an injected coherent signal is an important area of research with a great variety of applications. Experiments with this special arrangement have been performed leading to different kinds of solutions (locked lasers, pulses, etc.) [Simpson *et al.*, 1997]. The behavior of the system can be qualitatively different depending on the choice of parameters: numerical experiments in three-dimensional models of lasers with injected signal (LIS), revealed different "routes to chaos" in different parameter regions [Tredicce *et al.*, 1985; Solari & Oppo 1994; Wieczorek *et al.*, 2000].

A good theoretical understanding of the underlying mechanisms governing the great variety of possible behaviors was required. An early attempt in this direction, [Solari & Oppo, 1994] aimed to approximate the three-dimensional rate equations for a class B laser in the vicinity of the parameter region where this system becomes a Hamiltonian system, by a more tractable two-dimensional averaged system [Guckenheimer & Holmes, 1983]. A detailed study of the invariant sets revealed that at the heart of this nonlinear system, the Hopf-saddle-node (HSN) bifurcation played as an organizing center.

In more mathematical terms, this local bifurcation arises when the linearization of the vector field has a degenerate fixed point with two purely imaginary and a simple zero eigenvalue. The unfolding of this bifurcation requires two parameters (the amplitude injection rate β and the injected signal detuning η), and four different variants known as Type (I–IV) have been studied [Guckenheimer & Holmes,

1983; Wiggins, 1991]; minimally all of these Types display curves of saddle-node and Hopf bifurcations of fixed points in parameter space, which are tangent at one point. For increasing cavity detuning $\theta > 0$ [Solari & Oppo, 1994] found that Types II, I and III may be visited (in that order).

The interest in a physical (and testable) application displaying the above qualitative changes close to the Hopf-saddle-node bifurcation, is not restricted to the determination of the well-known invariant sets which result from normal-form analysis (saddle-node, primary and secondary Hopf bifurcations). Global behavior not present in the usual unfolding of HSN singularity has recently been studied as a primary source for chaotic behavior in LIS.

For example, in the large cavity detuning regime (corresponding to Type III of HSN) [Zimmermann *et al.*, 1997] showed the occurrence of Shilnikov homoclinic orbits [Šhil'nikov, 1965] to either saddle-focus fixed points (locked solutions). Further, as the detuning is decreased the transition from Type III to Type I showed that the homoclinic orbits to a fixed point, turns *at the critical* θ *where the HSN Type changes* to a homoclinic tangency to the periodic orbit of HSN [Zimmermann *et al.*, 2001]. This novel behavior opens the possibility that this physical system may become an ideal test-bench for new global bifurcation scenarios.

The present work completes the above series of studies of bifurcations of the laser with injected signal in the neighborhood of the HSN singularity. We numerically analyze the weak cavity detuning regime for a fixed value $\theta = 0.5$ (in adequate units), where Type II HSN is expected. The small-detuning case is particularly relevant for applications, since a natural ambition when constructing laser cavities is to obtain low detunings. Long-time behavior depending on the amplitude and the frequency shift of the applied signal is studied. The main bifurcation structure consists of a (secondary) Hopf bifurcation on the periodic orbit associated to the HSN bifurcation. We have analyzed in detail the resonance structure which reveals a rich interaction with other bifurcations *not* present in the usual HSN scenario. We find that the Arnold tongues are truncated by another (secondary) Hopf bifurcations of periodic orbits. These in turn are born in an Andronov global bifurcation at the saddle-node of fixed points (saddle-node infinite period bifurcation) [Kuznetsov, 1997]. Another particular behavior is that inside the Arnold tongues we also find homoclinic bifurcations to a saddle fixed point corresponding to the off-state of the laser. Finally we show how the Arnold tongues of increasing winding number, with all its associated bifurcations, *accumulate* towards the Hopf-saddle-node bifurcation point.

In the previous studies on the global bifurcations in LIS, a combination of the HSN singularity together with a global reinjection resulted in a proper framework for understanding the laser dynamics. However, in Type II we find a new possible complication which involves a heteroclinic cycle with the off-state. This will be left as a conjecture and discussed in Sec. 5.

The paper is organized as follows. In the next section we review the representative equations for LIS, together with the unfolding of the HSN bifurcation. In Sec. 3, the resonance structure is described, while Sec. 4 discusses the Andronov global bifurcation occurring in this laser, and its interaction with other bifurcations. Finally, a global outlook and discussion is given in Sec. 5.

2. Equations for the Laser with Injected Signal

The model for a laser system is given in terms of the Maxwell–Bloch equations. In a great variety of lasers, the decay times associated with the population inversion and the electric field have different time scales, allowing for the adiabatic elimination of the fast decaying polarization variable (class B) [Solari & Oppo, 1994]. The rate equations in a reference frame rotating with the injected signal may be written as

$$\begin{aligned} \frac{dE}{dt} &= EW + i(\theta W + \eta)E + \beta\,, \\ \frac{dW}{dt} &= A^2 - \chi W(1 + g|E|^2) - |E|^2\,, \end{aligned} \tag{1}$$

where E is the complex envelope of the electric field and W is proportional to the population inversion. θ represents the detuning between the atomic and the nearest eigenfrequency of the cavity, A is proportional to the amount of pumped atoms, $\chi \geq 0$ is proportional to the decay time of the population inversion and g is inversely proportional to $1+\theta^2$. η is the detuning of the perturbation frequency and the unperturbed laser operating frequency and $\beta \geq 0$ is the intensity of the injected signal. The relationship

between the parameters used in this model and the parameters in the Maxwell–Bloch equations can be found in [Solari & Oppo, 1994]. The model can be justified for small signal intensity ratio, $\beta/A^2 \ll 1$, and it has been argued that it can be successfully applied beyond this limit [Oppo *et al.*, 1986]. Our present study centers in this limit and in some cases we have explored a region beyond this limit in order to understand the fate of some invariant sets.

Solari and Oppo [1994] performed a reduction of the three-dimensional model by averaging over the fast relaxation oscillation motion, reducing the dynamics to a two-dimensional system. In this way, the difficulty of finding analytic expressions for most of the local bifurcations is simplified. A close analysis of the singularities of this model, reveals that the system organizes around the codimension-2 Hopf-saddle-node (HSN) local bifurcation. One finds that after a suitable change of coordinates one may arrive to its normal form representation [Guckenheimer & Holmes, 1983]:

$$\begin{aligned} r' &= (\mu + az)r + \mathcal{O}(3)\,, \\ z' &= \nu + br^2 - z^2 + \mathcal{O}(3)\,, \\ \zeta' &= \omega_0 + az + \mathcal{O}(2)\,, \end{aligned} \tag{2}$$

where a, b, $\omega_0 \neq 0$ and μ and ν are the bifurcation parameters, all functions of the laser parameters. The signs of a and b classify different types of flows: Type I for ($a > 0, b > 0$), Type II for ($a < 0, b > 0$), Type III for ($a > 0$, $b < 0$), Type IV for ($a < 0$, $b < 0$).

One of the main achievements of the Solari and Oppo average model is that they have established that the actual laser with injected signal operation is controlled by the cavity detuning parameter θ in the following way:

$$\begin{aligned} &\text{Type II} : 0 < \theta < 1\,, \\ &\text{Type I} : 1 < \theta < \sqrt{3}\,, \\ &\text{Type III} : \sqrt{3} < \theta\,. \end{aligned}$$

We refer the reader to [Zimmermann *et al.*, 2001] for a detailed account of the normal form computations for the three-dimensional LIS equations (1), where the above results are validated up to order $O(\chi^2)$, for

$$\begin{aligned} a(\theta) &= (1 + gA^2)\frac{(\theta^2 - 1)}{4\theta}\chi + O(\chi^2)\,, \\ b(\theta) &= -(1 + gA^2)\frac{(1 + \theta^2)(\theta^2 - 3)}{8\theta}\chi + O(\chi^2)\,, \\ \omega_0 &= \sqrt{2}A + O(\chi^2)\,. \end{aligned} \tag{3}$$

In terms of the laser parameters we find from [Solari & Oppo, 1994]:

$$\begin{aligned} \mu(\beta, \eta) &= \theta\left(\frac{2}{1+\theta^2} - \frac{\chi}{\beta\theta\sqrt{1+\theta^2}}\right), \\ \nu(\beta, \eta) &= 2\left(\frac{\beta\sqrt{1+\theta^2} + \eta}{\beta(1+\theta^2)}\right). \end{aligned} \tag{4}$$

The main characteristics of each Type of flow may be summarized as follows. A saddle-node bifurcation occurs for $\nu = \nu_{\rm sn} = 0$, where a pair of saddle-focus fixed points are born at $(r, z) = (\pm\sqrt{\nu}, 0)$. These fixed points may as well bifurcate in a Hopf bifurcation along a parabola in parameter space, $\nu = \nu_{\rm Hopf} = \mu^2/a^2$. The periodic orbit will be at $z_{\rm Hopf} = -\mu/a$ and its radius is given by $r^2_{\rm Hopf} = (\mu^2/a^2 - \nu)/b$. The main differences between Types I–III, lies in the region of existence and stability of the periodic orbit. In Type III the periodic orbit always coexists with the fixed points ($\nu > \mu^2/a^2 > 0$), while in Type I the periodic orbit exists before the creation of the fixed points (for $\nu < 0$, $r_{\rm Hopf} > 0$). Type II is similar to Type I, but the stability of the periodic orbit may change. A degenerate (secondary) Hopf bifurcation occurs on the semiaxis $\mu = 0$, $\nu < 0$, where the periodic orbit becomes a center.

Addition of appropriate third-order terms to the normal form (2), in general breaks this degeneracy and results in a bifurcation to a torus. The fate of the torus will depend on the perturbation applied to (2) and results concerning this Type are unknown. Kirk [1991] has analyzed these kind of perturbations for Type III, where the secondary Hopf bifurcation occurs in the semiaxis $\mu = 0$, $\nu > 0$, coexisting with the fixed points. In her analysis she found that the torus breaks-up in Arnold tongues [Arnold, 1983], which in turn end up as *resonances of another secondary Hopf bifurcation.* Below a similar scenario will hold.

In the present work we will investigate the small detuning regime $0 < \theta < 1$ corresponding to Type II. In terms of bifurcations and periodic orbit organization, the most prominent feature is the (secondary) Hopf bifurcation of periodic orbits associated to the HSN singularity. This will be one of our main objects of study, where we will discuss the interaction of its resonances with other bifurcations not present in the (local) normal-form analysis.

3. Bifurcation Set for Small Detuning

We have integrated numerically Eqs. (1) with fixed parameters $A = 1$, $\chi = 0.3$ and $g = 0$.[1] Most computations were done with the AUTO97 [Doedel *et al.*, 1997] continuation package, in the parameters (β, η) and $0 < \theta = 0.5 < 1$. In general, the locus in parameter space of a particular bifurcation will be presented as points, representing the actual computation performed. To guide the reader we have selected different colors for each type of bifurcation.

Given the complexity of the full bifurcation set found, we will introduce in steps the different invariant sets and their bifurcations. Impatient readers may refer to Fig. 19 for the full bifurcation set discussed in this paper.

3.1. *Invariant sets close to the Hopf-saddle-node bifurcation*

We begin our numeric exploration with the locus of the saddle-node, Hopf and Hopf-saddle-node bifurcations of fixed points. These may be explicitly computed, with the relevant equations being:

1. The fixed point equation may be reduced to,

$$\begin{aligned}(1+\theta^2)Y^3 - 2[A^2(1+\theta^2)+\chi\eta\theta]Y^2 \\ + [A^4(1+\theta^2)+2A^2\chi\eta\theta+\chi^2\eta^2]Y \\ - \chi^2\beta^2 = 0\,,\end{aligned} \tag{5}$$

   a cubic polynomial in $Y = |E|^2$.
2. The saddle-node condition, i.e. when one of the eigenvalues of the Jacobian is zero:

$$\begin{aligned}3(1+\theta^2)Y^2 - 4[A^2(1+\theta^2)+\chi\eta\theta]Y \\ + A^4(1+\theta^2)+2A^2\chi\eta\theta+\chi^2\eta^2 = 0\,.\end{aligned} \tag{6}$$

3. The Hopf condition (i.e. when two (complex conjugated) eigenvalues of the Jacobian are pure imaginary) reads:

$$\begin{aligned}(1+\theta^2)Y^3 - [3A^2(1+\theta^2)+\chi^2(\theta^2-3) \\ + 2\eta\chi\theta]Y^2 + [3A^4(1+\theta^2)+A^2[(\theta^2-5)\chi^2 \\ + 4\eta\chi\theta] + 2\chi^4 + \theta\chi^3\eta + \eta^2\chi^2]Y - [(1+\theta^2)A^6 \\ + 2A^4(\eta\chi\theta-\chi^2) + A^2(\eta^2\chi^2+\chi^4)] = 0\,.\end{aligned} \tag{7}$$

The fixed point equation reveals that there are regions of one or three fixed points, separated by saddle-node bifurcations. The simultaneous solution of (5) and (6) (the fixed point equation will then have a double root) gives the locus of the saddle-node curve, while solution of (5) with (7) gives the locus of the Hopf curve. When all three equations are simultaneously satisfied there is a tangency point where the Hopf-saddle-node occurs [Zimmermann *et al.*, 2001],

$$\begin{aligned}\eta_{\rm hsn}(\theta) &= -\frac{(1+\theta^2)}{2\theta}\left(1-\frac{1}{4\theta^2A^2}\chi^2\right)\chi + \mathcal{O}(\chi)^4\,, \\ \beta_{\rm hsn}(\theta) &= \frac{A\sqrt{1+\theta^2}}{2\theta}\left(1-\frac{(1+\theta^2)}{4\theta^2A^2}\chi^2\right)\chi + \mathcal{O}(\chi)^4\,.\end{aligned} \tag{8}$$

A typical bifurcation set displaying these bifurcations is shown in Fig. 1. Inside the "triangle" shaped region, three fixed points exists, while outside this region only one fixed point remains. Let us label the fixed points in region 1 as: A stable, B unstable and C saddle. A pair of the above fixed points are annihilated crossing the sides of the triangle: moving into region 4, B and C collide, while entering region 6 or $(3, 3')$, A and B annihilates leaving in these regions only the fixed point C.[2] In physical terms, *locking* behavior (output frequency tuned to that of the injected signal) occurs whenever the laser is operated in either regions $(1, 4, 5)$, where a stable fixed point exists. On the other hand, fixed point C exists in all regions except 4 in Fig. 1 and is approximately situated in $(|E|, W) \approx (0, A^2/\chi)$ for $\beta \ll 1$, which corresponds to the laser-off state. In all regions of interest it is a saddle fixed point.

The (primary) Hopf bifurcation occurs on either fixed point A or B, creating a periodic orbit *transversal* to the $W = 0$ plane, which will be referred to as T in what follows. This orbit corresponds to the undamped relaxation oscillation [van Tartwijk & Lenstra, 1995], whose main characteristic is that the phase of the electric field remains bounded. A closed circuit in parameter space around the HSN point reveals that moving from region 1 to

[1] In real lasers $g \,\varepsilon [0, 1]$. However, the qualitative features of the bifurcations around the HSN bifurcation will not change if g is kept small. In [Zimmermann *et al.*, 2001] it is found to slightly modify the second-order coefficients in the HSN normal form.

[2] Notice that choosing a path far out from the "triangle" shaped region, we have to identify fixed point C in regions $(6, 3, 3')$ with fixed point A in region 4.

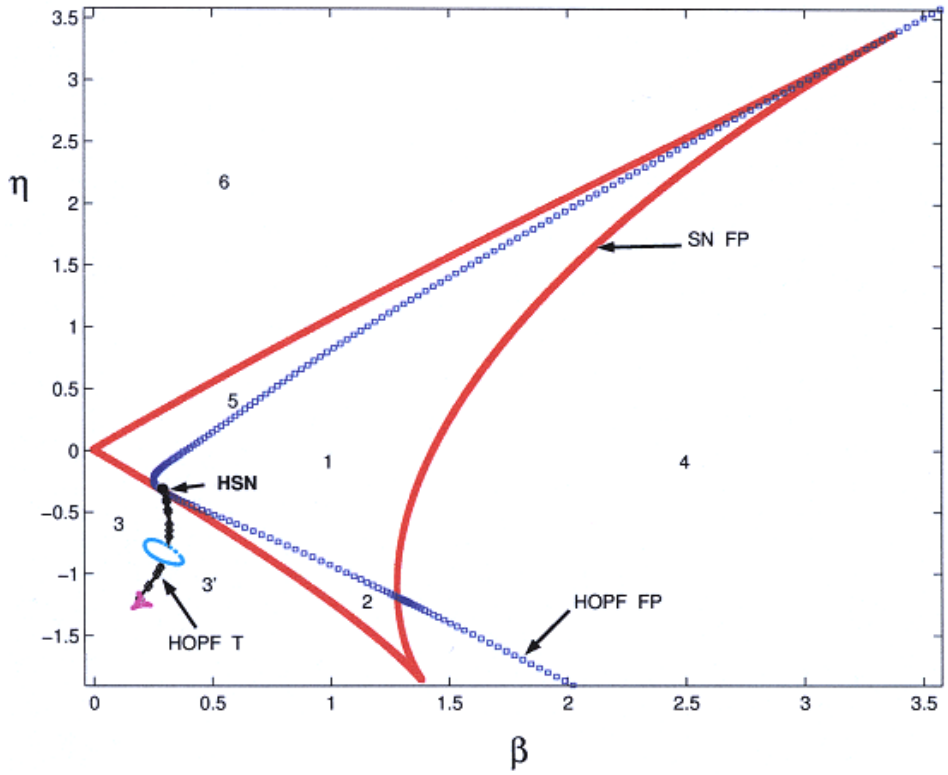

Fig. 1. Numerical bifurcation set in parameters (β, η) for Type II. Red line: saddle-node of fixed points (SN FP). Blue line: Hopf bifurcation of fixed points (HOPF FP). The secondary Hopf bifurcation of transversal periodic orbits (HOPF T) separates regions 3 and 3′.

region 5, the unstable node B becomes a saddle and creates an unstable T orbit. This orbit exists up to region 3, where it suffers a (secondary) Hopf bifurcation when crossing to region 3′, creating an unstable transversal torus. The remaining stable T periodic orbit continues to exist up to region 2, when it dies in a (primary) Hopf bifurcation with fixed point A.

To complete the main invariant sets present in regions 3 and 3′, we have to include another periodic orbit. For sufficiently small β we find from (1) that for $W \approx 0$, $|E| \approx A$ and the phase $\arg(E(t)) = \eta t$, which corresponds to the *cw* (continuous-wave) laser solution [van Tartwijk & Lenstra, 1995] with an unbounded electric field phase. As this orbit lies approximately coplanar to the $W = 0$ plane, it will be referred to as L, the *longitudinal* orbit. For sufficiently small (η, β), this orbit can be easily shown to be stable. However we find that the period of L diverges at the saddle-node bifurcation of fixed points where the orbit disappears. This global bifurcation is known as Andronov or saddle-node infinite-period bifurcation [Kuznetsov, 1997], and will be addressed in more detail in Sec. 4. We remark that the stability of L close to the Andronov bifurcation depends on the stability of the saddle-node fixed point, thus on which side of the HSN point one is: in region 3′ the orbit is unstable, while in region 3 it is stable. From this, it is clear that at least a local bifurcation to L is required. Below we will show that a new secondary Hopf bifurcation on L occurs inside region 3′.

In summary, we find that fixed points A and B together with the transversal periodic orbit T correspond to the Type II Hopf-saddle-node scenario proposed by the normal-form analysis in the previous section. The periodic orbit L is also an integral part of the bifurcation set in LIS, and we will show in the next section how the interaction of bifurcations between these two periodic orbits organize the resonance structure.

3.2. *Bifurcations of transversal periodic orbits*

We begin with a general observation for the existence boundary of transversal T orbit born at the Hopf bifurcation of fixed points. For a fixed value of η, we find for the continuation of this orbit for decreasing β, its period diverges at a critical $\beta \approx 0.05$,

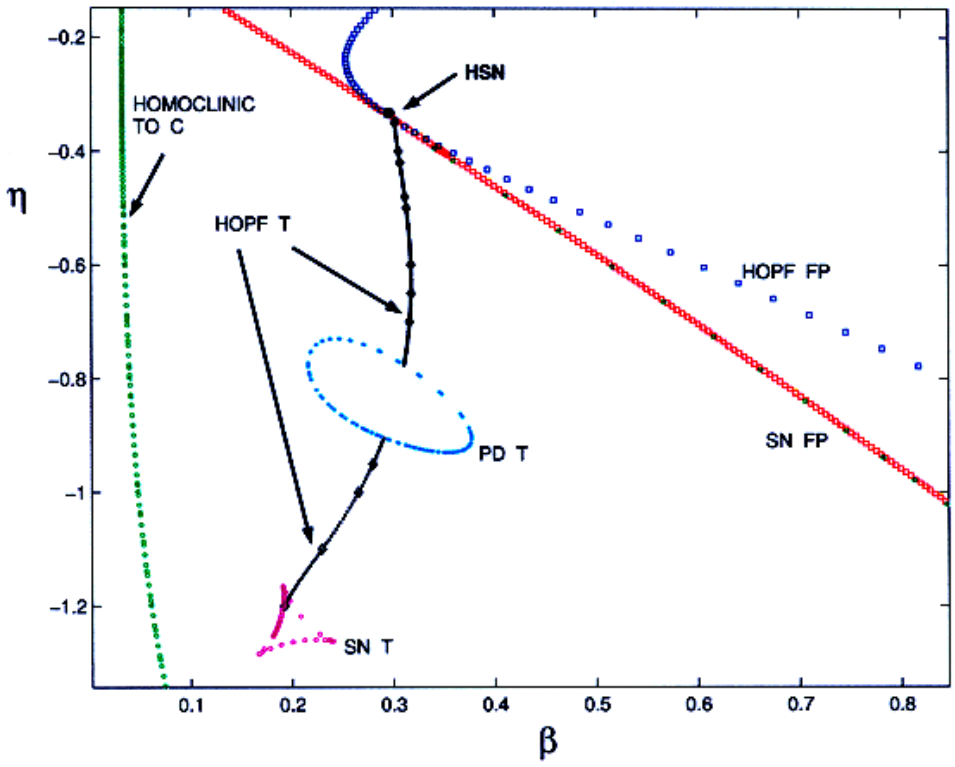

Fig. 2. Partial numerical bifurcation set showing the homoclinic to C fixed point and the first resonances of the transversal secondary Hopf bifurcation. Saddle-node bifurcation of transversal periodic orbits (SN T) and period doubling bifurcation of transversal periodic orbits (PD T) are indicated.

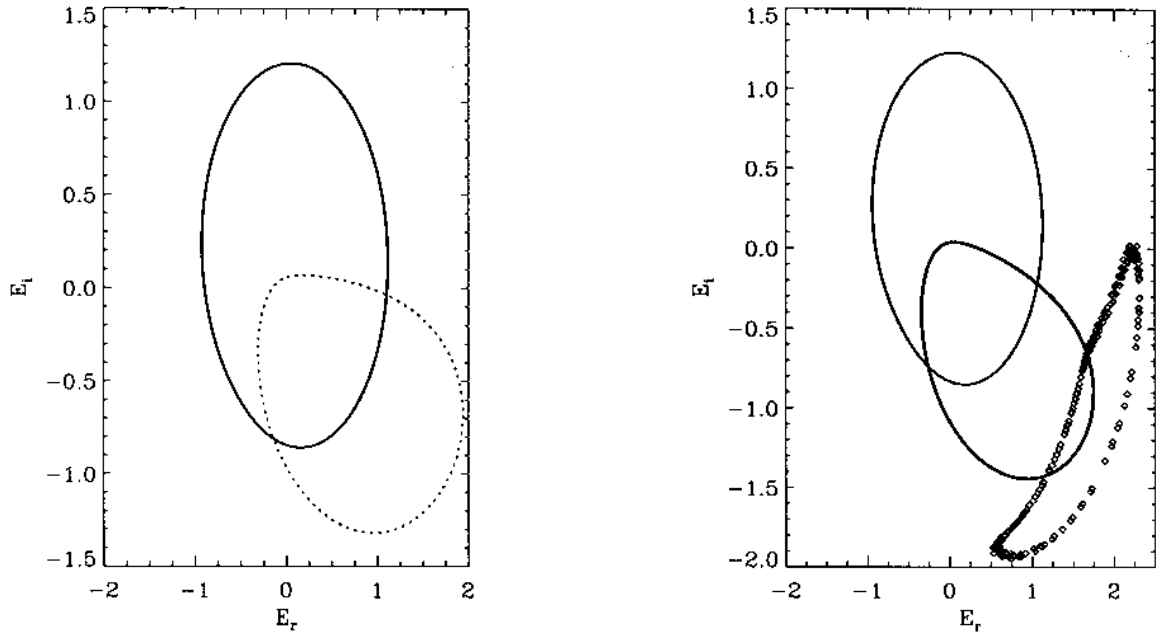

(a) (b)

Fig. 3. Phase portrait in $(E_r = \mathrm{Re}(E), E_i = \mathrm{Im}(E))$ of periodic orbits in the neighborhood of the (secondary) Hopf bifurcation of T. Solid lines: stable orbits, dot lines: unstable trajectories. $\eta = -1$. (a) $\beta = 0.24$, (b) $\beta = 0.28$. The torus created is an unstable one.

for an interval of η close to 0, where a homoclinic orbit to fixed point C occurs. Figure 2 shows the locus of this global bifurcation in parameter space, while Fig. 8 shows the typical period versus β behavior. This bifurcation is found not to depend on θ, and was found up to Type III regime. We leave for Sec. 4 the discussion of how this bifurcation is related to the Andronov bifurcation producing L.

In Fig. 3(a) we display the main invariant sets for the parameter region bounded by the homoclinic to C and the secondary Hopf bifurcation. We have the stable longitudinal orbit L (which lies approximately on $|E| \approx A = 1$, $W \approx 0$), together with the unstable transversal orbit T. This orbit has a large variation in the inversion population W, and a bounded electric field phase (the phase does not make a complete turn as L does). Crossing the secondary Hopf bifurcation T and entering region $3'$, we find that T becomes stable and an unstable invariant torus is created. Figure 3(b) shows the invariant sets, where only the intersections of the quasiperiodic orbit with the $W = 0$ plane are shown. A time series of the intensity $|E|^2$ on this solution is shown in Fig. 4.

It is well known that in generic systems, quasiperiodic motion may suffer resonance phenomena. Local analysis [Arnold, 1983] around the Hopf bifurcation reveals that whenever the ratio of the two competing frequencies is rational, the quasiperiodic motion may disappear and periodic orbits arise. These orbits may be classified by an integer number of p turns following the primary or bifurcating orbit (T in this case), and another integer

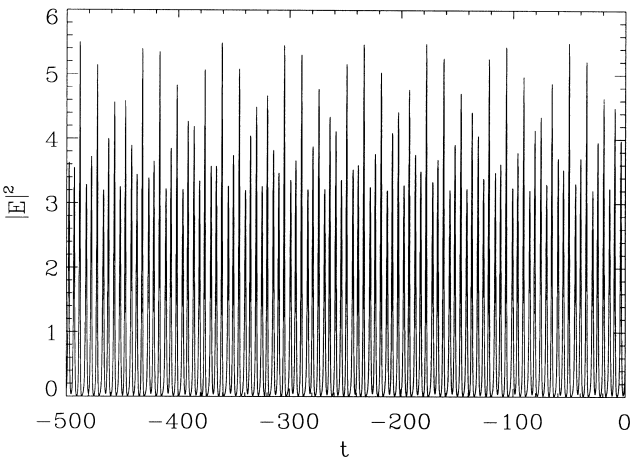

Fig. 4. Intensity ($|E|^2$) versus time for the unstable transversal torus created in the Hopf bifurcation of T periodic orbits. $\eta = -1$, $\beta = 0.28$.

number q which denotes the number of turns made around the primary orbit, before closing on itself. Precisely on the (secondary) Hopf bifurcation the nontrivial Floquet multipliers are on the unit circle at $e^{\pm i2\pi p/q}$. A general result shows that in the *weak resonances* case $q > 4$ these periodic orbits are born in saddle-node pairs, and in a two-parameter space they trace a "tongue" (known as Arnold tongue) with the tip lying on the (secondary) Hopf bifurcation. In phase space the periodic orbits are *phase locked* solutions on the torus. On the other hand the case $q \leq 4$ are known as *strong resonances* and do not correspond to "strict" Arnold tongues. A detailed account of the unfoldings of each strong resonance may be found in [Kuznetsov, 1997].

In Fig. 5 we display the resonance structure for $1/q$, $q = 1, \ldots, 12$, where the saddle-node of the resonant periodic orbits have been continued in parameter space. Of course in general one expects a countable number of tongues, one for each rational p/q. We will show below the location of other resonances with $p \neq 1$. We find that the tongues corresponding to $q > 4$ behave like standard Arnold tongues, while $q = 1$, 2, 3, 4 behave in a different way as expected. Resonance $q = 4$ is well known not to finish in a cusp singularity (compare with [Kirk, 1991]), while resonance $q = 3$ does not even finish in a cusp bifurcation (see below for a detailed description of this resonance). For lower η, resonance $q = 2$ arises whenever the nontrivial Floquet multipliers of the primary periodic orbit (T) collide in a doubly degenerate -1 eigenvalue. In this case, we find in parameter space the Hopf bifurcation is interrupted by an "isola" of period-doubling bifurcations (PD T in Fig. 5). For even lower η we find that the Hopf bifurcation is finally interrupted when the two nontrivial Floquet multipliers become degenerate at $+1$. In this case a saddle-node bifurcation of periodic orbits occurs (SN T in Fig. 5), and in fact a Takens–Bogdanov [Kuznetsov, 1997] singularity takes place. In Sec. 3.4 we discuss this with more detail.

The organization of the tongues in parameter space shows that for increasing q, the resonances appear to accumulate *towards* the HSN singularity. This may be easily understood by a simple analysis from the HSN normal form. Truncating the normal form (2), the eigenvalues of the Hopf periodic orbit (corresponding to T) at the (degenerate) secondary Hopf bifurcation $\mu = 0$, $\nu < 0$ are $\lambda_{1,2} = \pm i\omega_1 = \pm i\sqrt{2a\nu}$. Using the expression of

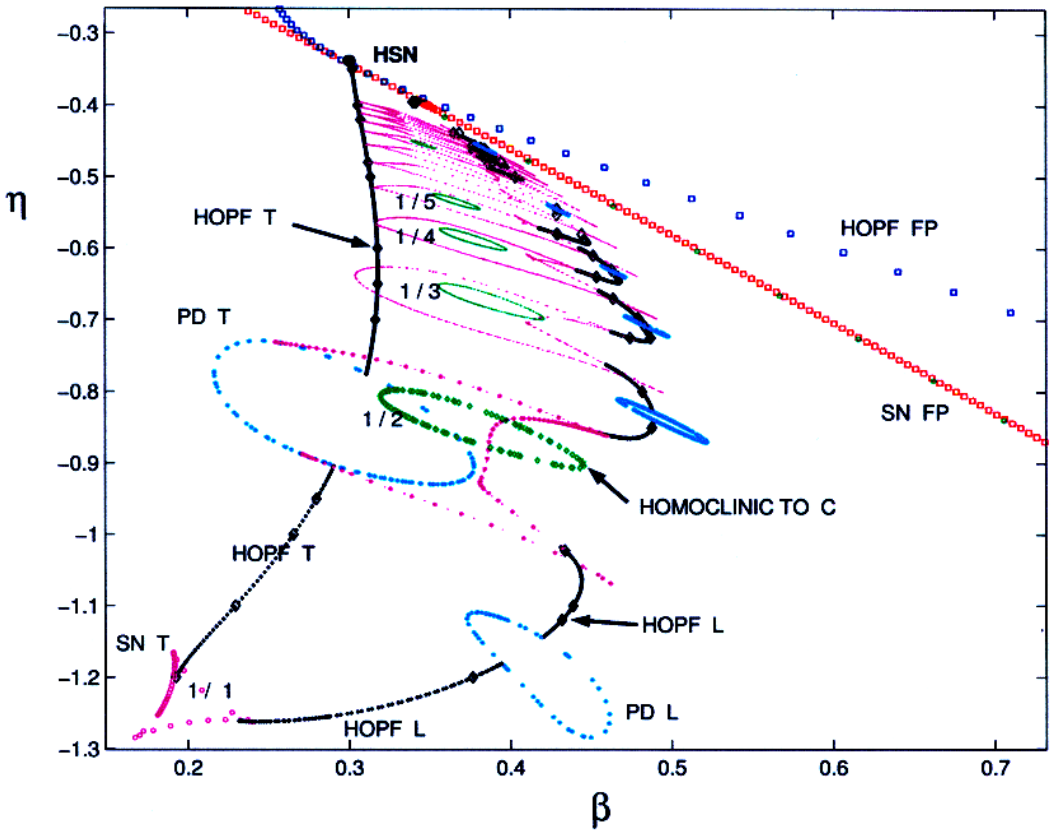

Fig. 5. Resonance structure for the transversal and longitudinal Hopf bifurcations, together with the homoclinic bifurcation to fixed point C. Period doubling bifurcations of longitudinal orbits (PD L) and Hopf bifurcations of longitudinal orbits (HOPF L) are displayed.

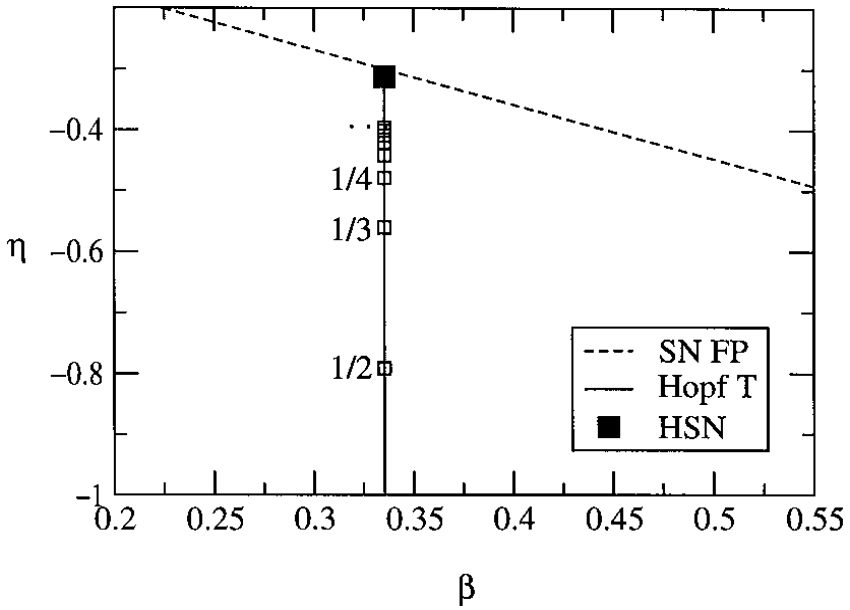

Fig. 6. Secondary Hopf bifurcation and its resonances $p/q = \{1/2, 1/3, 1/4, \ldots\}$ from an estimation of the HSN normal form (2) using LIS parameters (β, η). The dashed line is the saddle-node of fixed points while the vertical line is the secondary Hopf bifurcation. Compare with Fig. 5 ($A = 1$, $\theta = 0.5$, $\chi = 0.3$).

$a(\theta)$ and ω_0 in (3) we may estimate the position of the resonances in parameter space solving

$$p\omega_0 = q\omega_1(\nu)\,, \tag{9}$$

for each pair of p, q. It is clear that moving on the secondary Hopf and approaching the HSN singularity ($\nu \to 0$), the typical secondary frequency ω_1 goes to zero, so a larger q is required to satisfy the resonance condition. Figure 6 shows the result of this estimation of the resonance condition using the approximate reparametrization of LIS (β, η) parameters in terms of HSN parameters (4):

$$\begin{aligned}\eta(\mu,\,\nu) &= \frac{(1+\theta^2)(\nu-2)\chi}{2(-2\theta+\mu(1+\theta^2)}\,,\\ \beta(\mu,\,\nu) &= \frac{\sqrt{1+\theta^2}\chi}{-2\theta+\mu(1+\theta^2)}\,.\end{aligned} \tag{10}$$

The resonance structure is very similar to the one identified by Kirk [1991], but for Type III Hopf-saddle-node. The main difference is that in this Type the invariant torus coexists with the two fixed point solutions, and the possible homoclinic/heteroclinic between them. Her main result was that the Arnold tongues accumulated for increasing winding number towards this homoclinic/heteroclinic bifurcation are presented for this particular Type. In our case, we observe that the accumulation of the tongues saddle-nodes is onto the Andronov global bifurcation, occurring at the saddle-node of fixed points.

3.3. *Structure and truncation of Arnold tongues*

A closer look at how the periodic orbits are organized inside each resonance $q > 2$ is very interesting. To fix ideas we take resonance $q = 3$ shown in Fig. 7. We have performed three constant-η parameter cuts displayed in Fig. 8, where the period of the orbits as a function of β is shown. In each panel the unstable T periodic orbit is seen to be born at $\beta \approx 0.05$ (with diverging period) in a homoclinic bifurcation to C, becoming stable at $\beta \approx 0.30$ in the (secondary) Hopf bifurcation. Also for low β we observe the stable L orbit which suffers

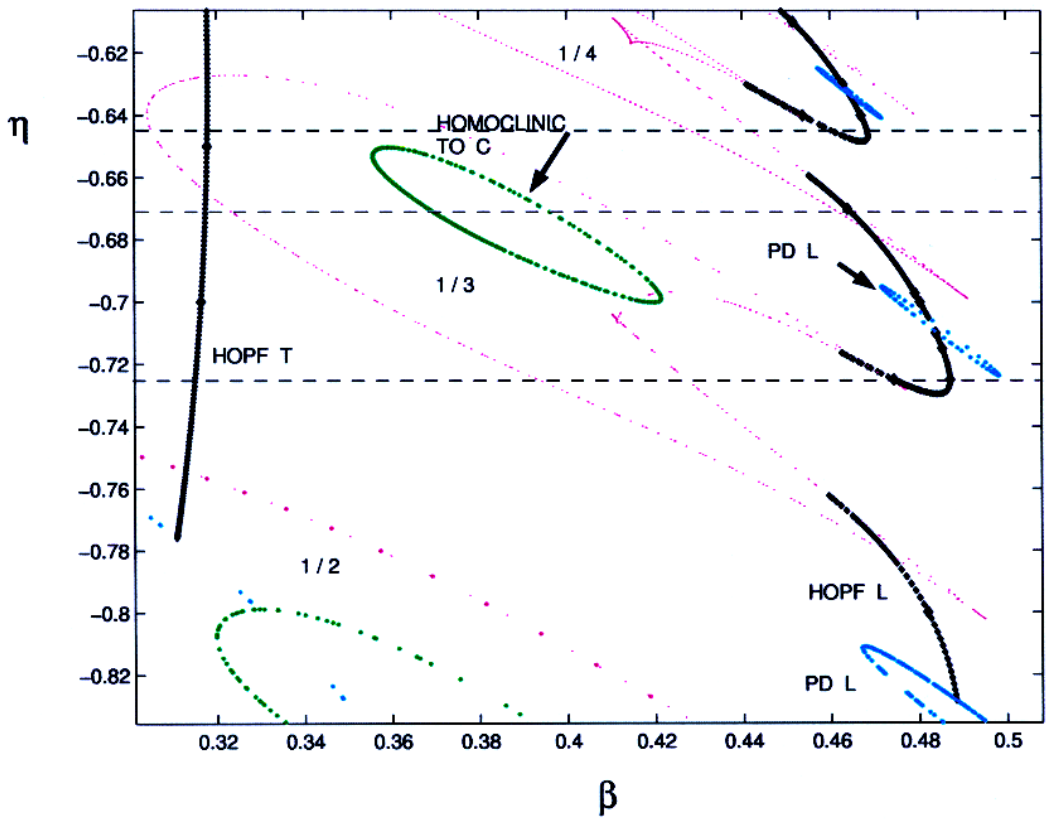

Fig. 7. Partial numerical bifurcation set around the 1/3 resonance. The horizontal lines are constant-η parameter cuts shown in Fig. 8.

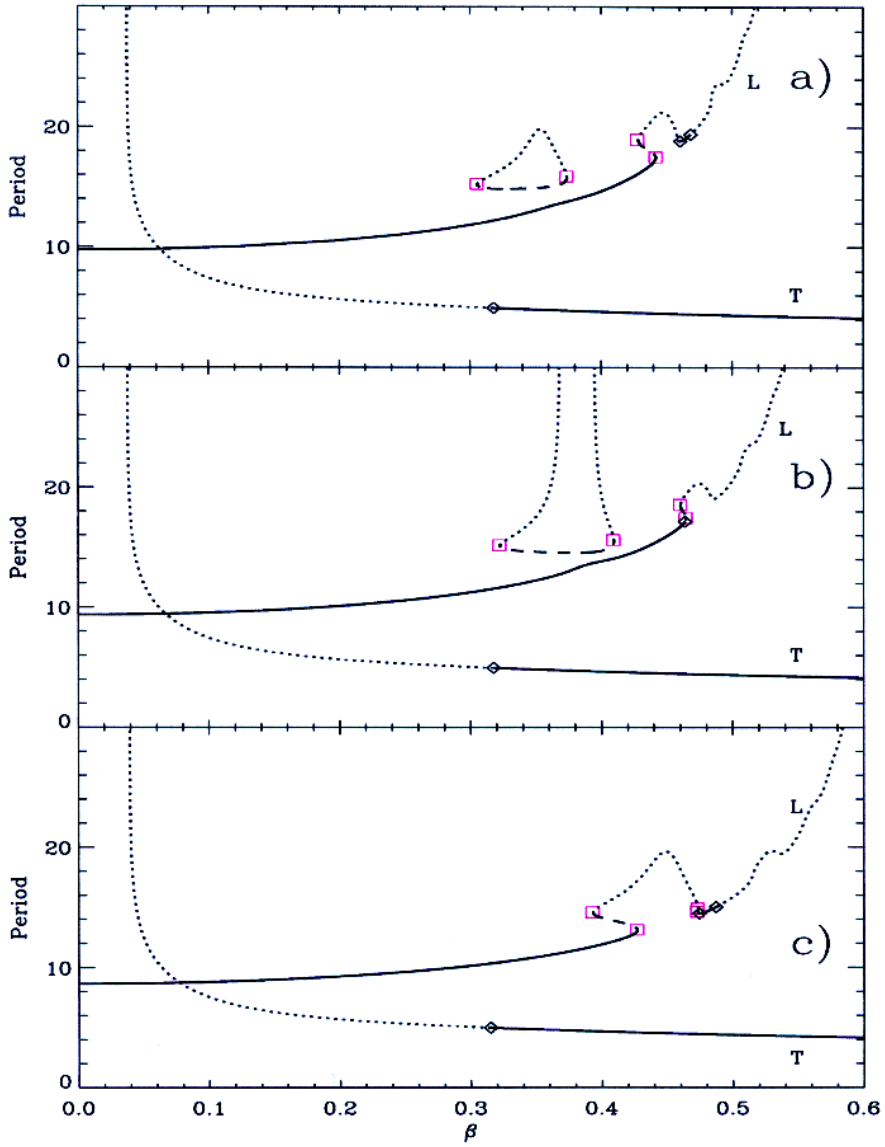

Fig. 8. Period versus β of periodic orbits inside the resonance $q = 3$. (a) $\eta = -0.645$: the two saddle-node bifurcations form an "isola" for the resonant periodic orbits close to the HOPF T bifurcation. (b) $\eta = -0.670$: the saddle branch of the isola "explodes" in period, creating two homoclinic bifurcations to C. (c) $\eta = -0.725$: the resonant branch of $q = 3$ periodic orbits merge with the L branch. Merging of the $q = 4$ resonance is also observed in (a). Solid line: stable orbit, dotted line: unstable orbit, dashed line: saddle orbit, □: saddle-node bifurcations of periodic orbits, ◊: hopf bifurcations of periodic orbits.

a number of saddle-node and Hopf bifurcations as β increases, and finally its period diverges as it approaches $\beta \approx 0.60$ the saddle-node infinite-period (Andronov) bifurcation.

In Fig. 8(a), close to the Hopf bifurcation of T, a saddle and unstable periodic orbits are born in a saddle-node bifurcation and collide at a higher β in a reverse saddle-node bifurcation. Both bifurcations correspond to the resonance boundaries shown in Fig. 7. For a slightly lower constant-η cut [Fig. 8(b)], we find that the unstable branch of the resonant periodic orbits "explodes" in period and two homoclinic bifurcations to C originate. These global bifurcations correspond to the isola of homoclinics to C observed in Fig. 7. Finally, in a cut further away from the $q = 3$ resonances of the Hopf of T [Fig. 8(c)], the homoclinics to C disappear and with the aid of another saddle-node bifurcation, the resonant periodic orbits "merge" with the L periodic orbit. Notice in Fig. 8(a) that resonance $q = 4$

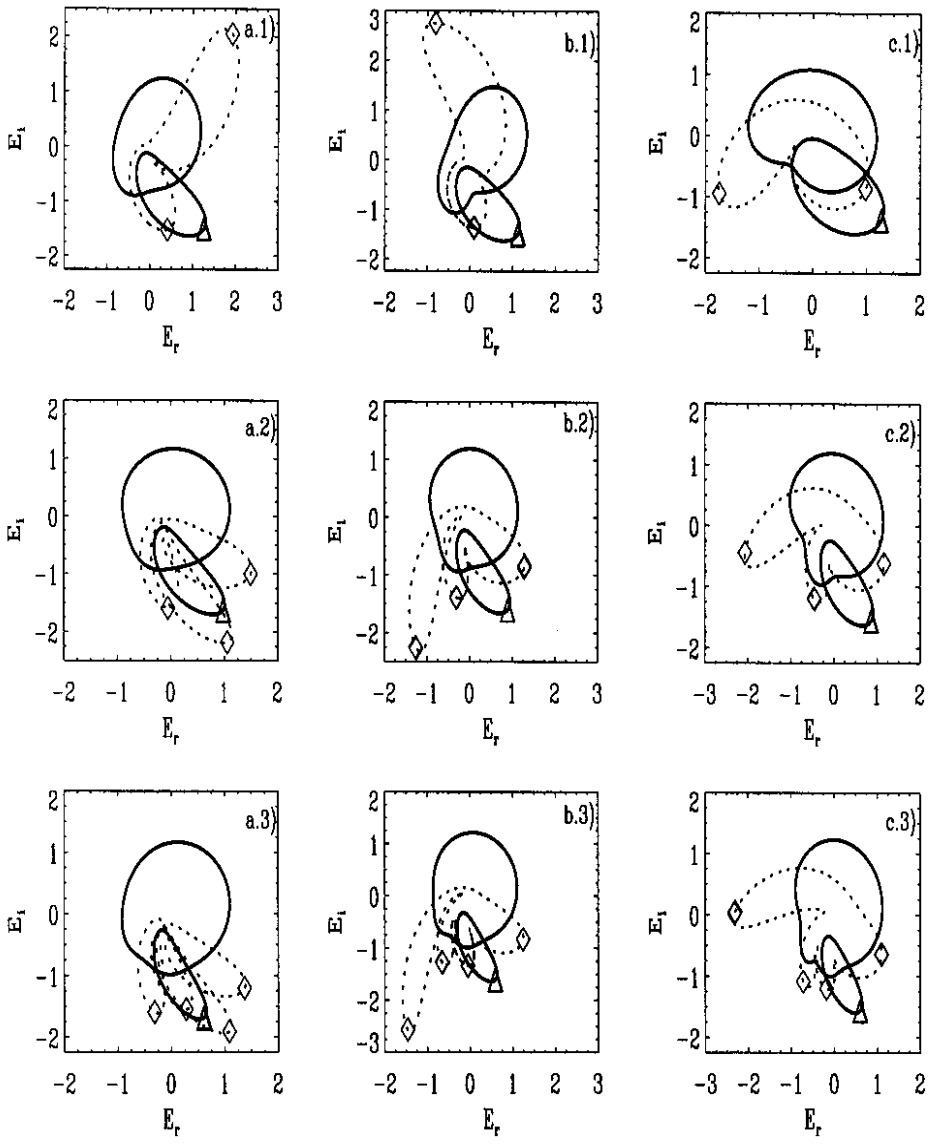

Fig. 9. Phase portraits of resonance orbits, together with T and L. Each row shows a continuation of a transversal $1/q$ resonance on the right column, ending in a longitudinal $1/q'$ orbit on the right column. For a clear visualization only the first row displays the whole resonance orbit, while only its intersections with $W = 0$ are shown in the subsequent rows. Resonance 1/2 (η, β): (a1) $(-0.77, 0.32)$, (b1) $(-0.83, 0.40)$, (c1) $(-1, 0.41)$. Resonance 1/3: (a2) $(-0.66, 0.32)$, (b2) $(-0.70, 0.38)$, (c2) $(-0.75, 0.44)$. Resonance 1/3: (a3) $(-0.565, 0.32)$, (b3) $(-0.60, 0.38)$, (c3) $(4, -0.64, 0.43)$. Solid lines: stable orbits, dot lines: unstable trajectories. Saddle orbits are not represented.

already merged to L. The above merging process of transversal resonances into the longitudinal periodic solution is observed for all resonances[3] $1/q$, $q > 2$.

One may wonder if there is a topological restriction for the merging process, as the transversal orbit (and its associated resonances) are *linked* in phase space to the longitudinal orbit L, as shown in Fig. 3. For this, in Figs. 9(a)–9(c) we illustrate a continuation of L, T and a resonant orbit in order to show how the linking of the transversal orbit remains as it merges to a longitudinal orbit.

In fact, close to the merging process, the longitudinal orbits L also bifurcates in a secondary Hopf bifurcation. Figure 10(a) illustrates the unstable L longitudinal orbit born at the Andronov bifurcation, bifurcating in a secondary Hopf bifurcation and creating a new unstable longitudinal torus

[3]Cases $q = 1$, 2 are more complicated involving a period-doubling bifurcation.

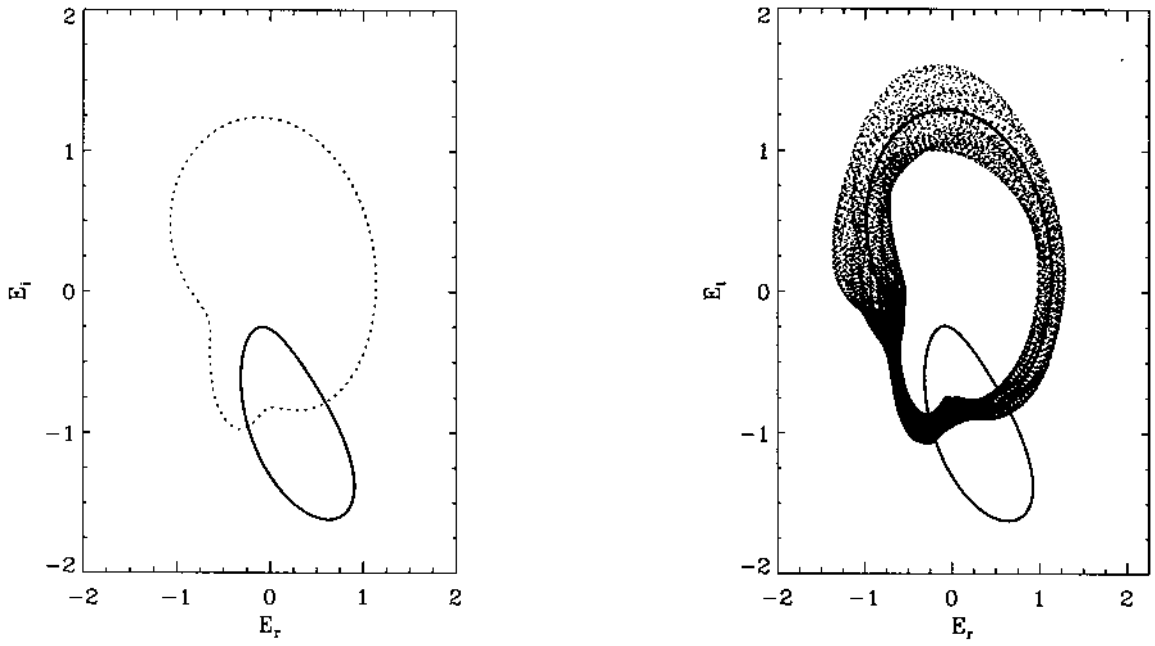

Fig. 10. Projections in the plane (E_r, E_i) of the orbits that exist on each side of the Hopf bifurcation of L periodic orbits. Solid lines: stable orbits, dot lines: unstable trajectories. $\eta = -0.8$. (a) $\beta = 0.485$, (b) $\beta = 0.477$. The torus created is unstable.

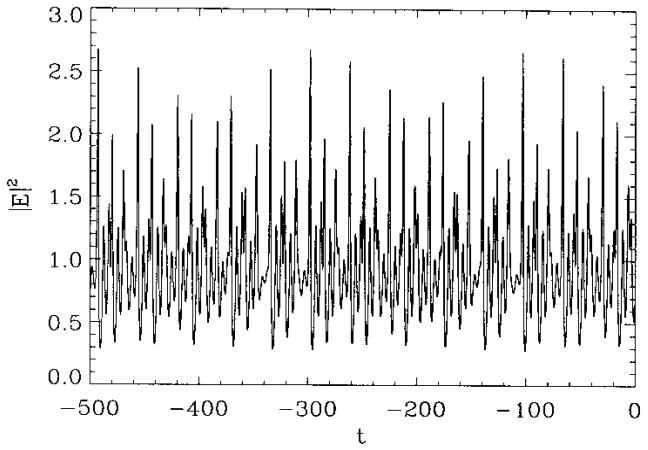

Fig. 11. Intensity versus time for the torus created at the Hopf bifurcation of L periodic orbits. $\eta = -0.8$, $\beta = 0.477$.

around L [Fig. 10(b)]. Notice also that the electric field intensity time series Fig. 11 is also quite different of that of Fig. 4.

The remarkable feature is the organization in parameter space of the above bifurcations. We have found that all $1/q$ transversal resonances, end up in a cusp bifurcation with another saddle-node bifurcation. The latter bifurcation is responsable for the merging described above, and on this branch a $1/q' = 1/1$ secondary Hopf bifurcation occurs on L. Continuation of the new Hopf bifurcation reveals that it suffers a $1/2$ resonance (with a period-doubling isola), before it ends at another $1/q' = 1/1$ resonance, corresponding to a transversal tongue $1/(q-1)$. This sequence of bifurcations is seen to occur for all the transversal $1/q$ resonances found.

The complete structure of the phase diagram of Fig. 5 has now been described and reveals a high organization which repeats as we approach to the HSN point. Several bifurcations not present in the local description of HSN take part in the dynamics: (a) we have the Arnold tongues which for increasing q accumulate to the Andronov bifurcation, (b) the secondary longitudinal Hopf bifurcation connecting subsequent transversal resonances, and (c) the homoclinic bifurcations to C (the off-state). The latter global bifurcations have a winding number in correspondence with the resonance it belongs. Thus in the limit close to HSN one expects an accumulation of homoclinic orbits to C of diverging winding number. Furthermore, most turns would follow the smaller loop T, as we approach HSN. This argument points to the possibility that another global connection between the HSN fixed point and the laser

off-state C exists. This has not been explored in detail and deserves further study (see Sec. 4 below).

3.4. *Homoclinics to periodic orbits*

As mentioned above, all strong resonances are known to possess more bifurcation structure than what we have pointed out. In particular, it is well known that unlike what happens in weak resonances, the saddle-node bifurcations of the tongues *do not* occur on the torus. Instead the invariant torus may grow as parameters change and eventually collide with one of the resonant periodic orbits. This would correspond to a *homoclinic bifurcation* to a periodic orbit, with the final destruction of the torus.

One example may be found in the intersection point of all 1/1 resonance points with the saddle-node bifurcation of periodic orbits. At this point one may expect a Takens–Bogdanov singularity [Kuznetsov, 1997] which is well known to have such a global bifurcation. Figure 12 shows an enlargement of the 1/1 resonance of the transversal T and longitudinal L orbits, where the diamonds indicate the approximate values where a homoclinic tangency was observed by direct numeric computation.

A closed loop around the TB point in Fig. 12 describes the main features. Moving from region B to F two periodic orbits are created, one saddle and one unstable. From F to G the secondary Hopf bifurcation creates an unstable torus, and the unstable periodic orbit becomes stable. In region G the radius of the torus grows as one approaches region H, and finally collides in a homoclinic bifurcation to the saddle periodic orbit. In Fig. 13 we illustrate a numeric computation of the stable and unstable manifolds of the periodic orbit T, showing clearly a homoclinic bifurcation. Notice that one expects homoclinic tangencies as one departs from the TB point. Finally, moving from H to B, the remaining periodic orbits disappear in a saddle-node bifurcation.

An analogous scenario holds for the TB point on the longitudinal orbits seen in Fig. 12, denoted homoclinic to L. In general, we also find TB bifurcation points in all $1/q' = 1/1$ resonances of L described above. We emphasize that this is

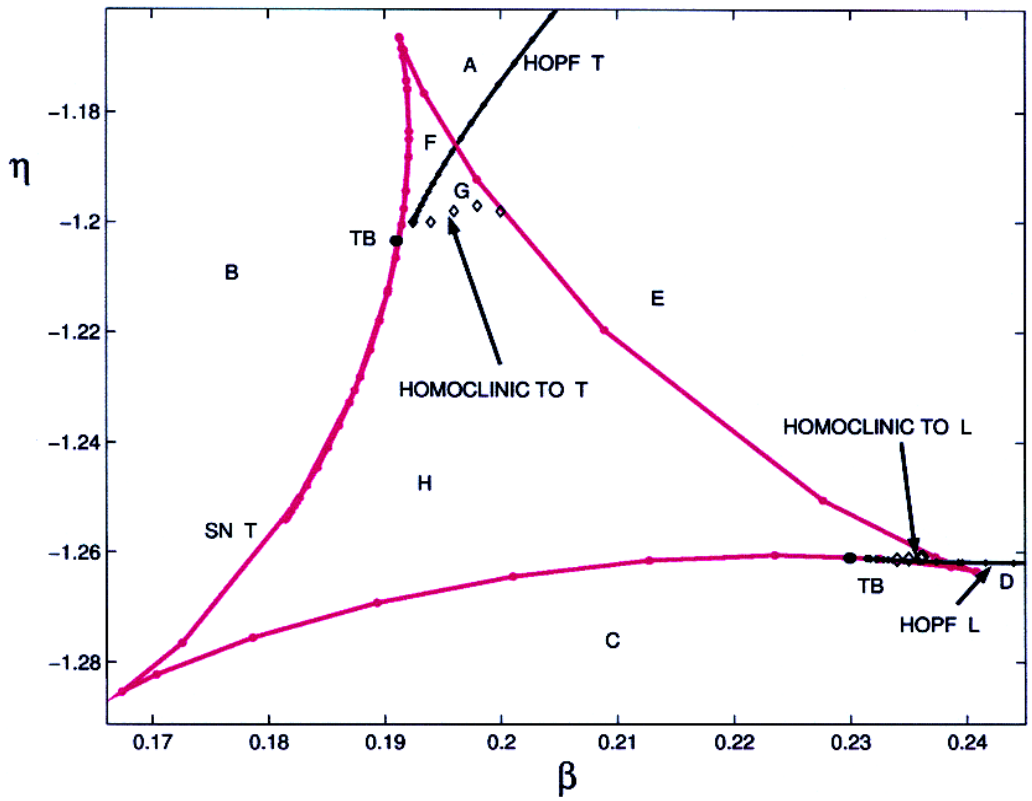

Fig. 12. Blowup of 1/1 resonance of transversal T and longitudinal L orbits. "◇" show the locus of homoclinic tangencies to T and L orbits.

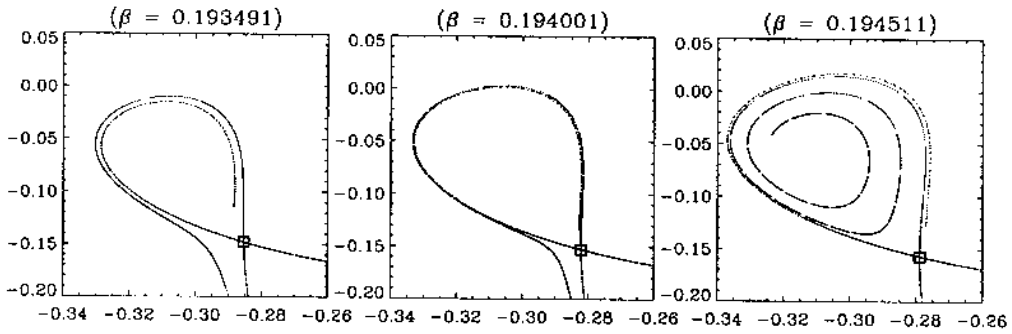

Fig. 13. Phase portraits of the Poincaré section $W = 0$ for the homoclinic bifurcation of the 1/1 transversal resonance, in the neighborhood of the homoclinic tangency. The saddle periodic orbit is at "□", and next we computed the stable and unstable manifolds ($\eta = -1.20$).

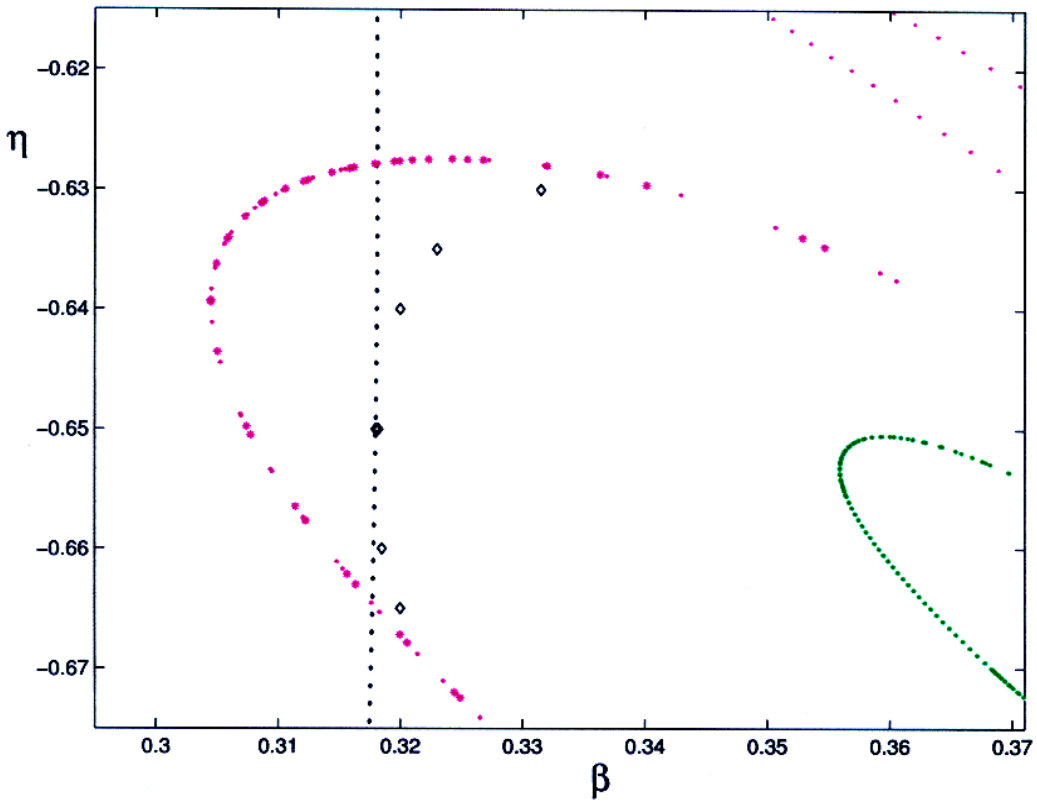

Fig. 14. Homoclinic bifurcation in 1/3 resonance. "◊" account for the homoclinic to the saddle T periodic orbit.

only an approximate view since at the TB point many other bifurcations originate (see [Hirschberg & Laing, 1995]).

A different homoclinic bifurcation to a periodic orbit is the one encountered inside the 1/3 resonance, see Fig. 14. This is a well established result from the normal form analysis of this bifurcation [Arnold, 1983; Kuznetsov, 1997]. The torus is found between the secondary Hopf and the homoclinic tangency. In this case, the torus grows and collides to a saddle period $q = 3$ orbit, which exists in an neighborhood of the T resonance point.

3.5. *Full resonance structure*

In general one expects a countable number of resonances for the breakup of quasiperiodic motion, one for each rational p/q. These may be organized following the Farey sequence [Aronson *et al.*, 1982], where between resonances p/q and p'/q' one always

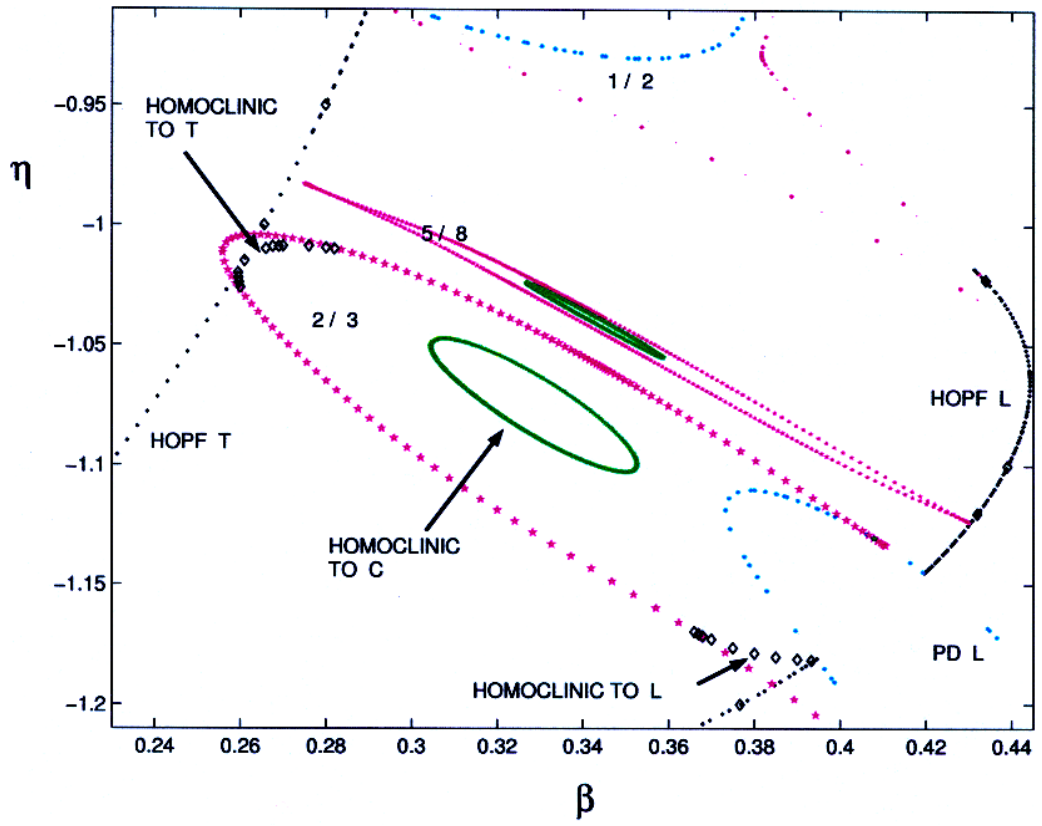

Fig. 15. Higher order resonance structure between 1/2 and 1/3 transversal resonances. Transversal resonance 2/3 becomes 1/2 resonant to orbit L, while transversal 5/8 resonance becomes a weak resonance to L.

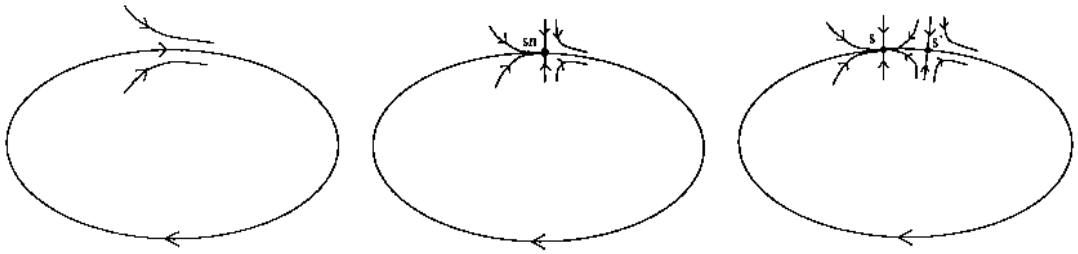

(a) (b) (c)

Fig. 16. One-parameter unfolding of Andronov bifurcation. Note that the stable manifold of the fixed points in (b) and (c) are two-dimensional in LIS.

finds resonance $(p + p')/(q + q')$. A full classification of all these resonances is quite complicated so we show the locus of two resonances with $p > 1$. In Fig. 15 we display two resonances in between the strong 1/1 and 1/2 of the transversal torus. They show basically the same structure, including the isola of homoclinic bifurcations to C and homoclinic bifurcations to T. One of them, the transversal 5/8 resonance, becomes a weak resonance in the neighborhood of the L torus. The other, a transversal 2/3 resonance becomes a strong 1/2 resonance in the neighborhood of the L torus. Notice also the homoclinic bifurcations to L and T periodic orbits found in this resonance.

4. Andronov Bifurcation

We now describe with some more detail the Andronov bifurcation found in LIS. In Fig. 16 we illustrate the phase portraits of the unfolding of this bifurcation in a one parameter cut. They

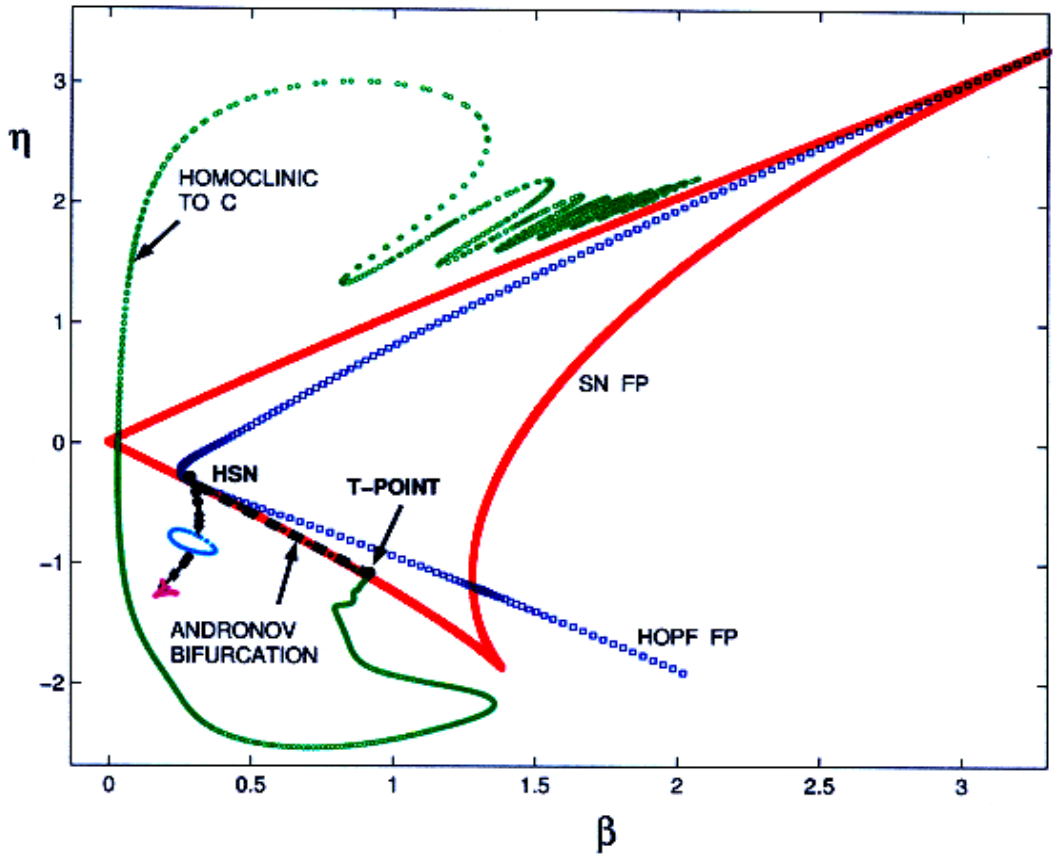

Fig. 17. Locus of homoclinic bifurcation to C fixed point, T-point, and Andronov bifurcation at the saddle-node of fixed points.

correspond to the Andronov–Lentovich[4] [Kuznetsov, 1997] bifurcation: a periodic orbit in the region of no fixed point collides in a homoclinic orbit with the saddle-node (SN) fixed point. At the bifurcation point, there exists an orbit leaving the central manifold, and returning after some finite time through the other central manifold of the saddle-node fixed point.

This bifurcation is quite representative in LIS and has been confirmed in several parameter regimes. The standard Adlers equation [van Tartwijik & Lenstra, 1995] is a one-dimensional example displaying this bifurcation. Also the two-dimensional averaged model of [Solari & Oppo, 1994], displays this bifurcation at the SN bifurcation of fixed points. This in fact motivated previous studies in global bifurcations, for in generic three-dimensional systems one expects that the global connection connecting the saddle-node to itself should break.

Results for Type III in [Zimmermann *et al.*, 1997] show that the Andronov global bifurcation exists for sufficiently small (β, η), but become degenerate at a point close to the HSN singularity, where a new codimension-2 bifurcation known as Shilnikov-saddle-node, occurs. At the bifurcation, the homoclinic orbit leaves through the central manifold the neighborhood of the saddle-node fixed point, but now returns through the *stable* manifold of the degenerate fixed point. Results for Type I $(1 < \theta < \sqrt{3})$ show that the Andronov bifurcation exists for the whole interval between $(\beta, \eta) = (0, 0)$ up to the HSN point. However on the other side of the codimension-2 point, homoclinic tangencies to T occur near the SN bifurcation of fixed points [Zimmermann *et al.*, 2001].

For Type II we display in Fig. 17 a continuation in parameter space of the Andronov bifurcation, approximated by continuation of a very high period L orbit. The locus of this global bifurcation

[4]In fact this bifurcation was studied by Andronov in 2-dimensions, while the n-dimensional case was solved by [Šhil'nikov, 1966]. However we keep the term Andronov bifurcation to the generic case.

starts at $(\beta, \eta) = (0, 0)$ and extends past the HSN point. The stability of the periodic orbit depends on the stable or unstable direction of the degenerate fixed point at the SN bifurcation. Therefore for $|\eta|$ small the stability of L is stable (region 3 in Fig. 1), while for values on the other side of the HSN point, L becomes unstable (region $3'$ in Fig. 1). In phase space, orbits born at this global bifurcation display a number of transversal oscillations ("bumps") in the region of phase space where the saddle-node fixed point (SN) disappeared. The number of these oscillations diverge as we approach from below the HSN bifurcation point, for in the neighborhood of this singular point there are *two* directions with extremely slow dynamics. Moving away from the saddle-node bifurcation, the transversal oscillations are observed to grow in phase space. We have shown in Sec. 3.3 how this periodic orbit is found in general to suffer saddle-node bifurcations corresponding to the resonance boundaries of the Arnold tongues, or a secondary Hopf bifurcation. This clarifies the integral role of the Andronov bifurcation in the complete bifurcation structure close to the HSN bifurcation point.

A new global bifurcation was found involving the Andronov bifurcation. For sufficiently negative η, the homoclinic orbit makes a global excursion which approaches the C fixed point. In parameter space, we find that the Andronov bifurcation collides at a point with the branch of homoclinic bifurcations to C. At the collision point a heteroclinic cycle between the saddle-node (SN) and C fixed point was found. That is, there is a heteroclinic connection leaving through the central manifold of SN and enters C through the stable one-dimensional manifold, and another connection which leaves through the two-dimensional unstable manifold of C, and enters back to SN through its two-dimensional stable(-center) manifold (see Fig. 18). This cycle is reminiscent to the T-point bifurcations found for two *nondegenerate* fixed points [Glendinning & Sparrow, 1986; Bykov, 1993; Zimmerman & Natiello, 1998]. So far, this degenerate heteroclinic system has not been studied in detail.

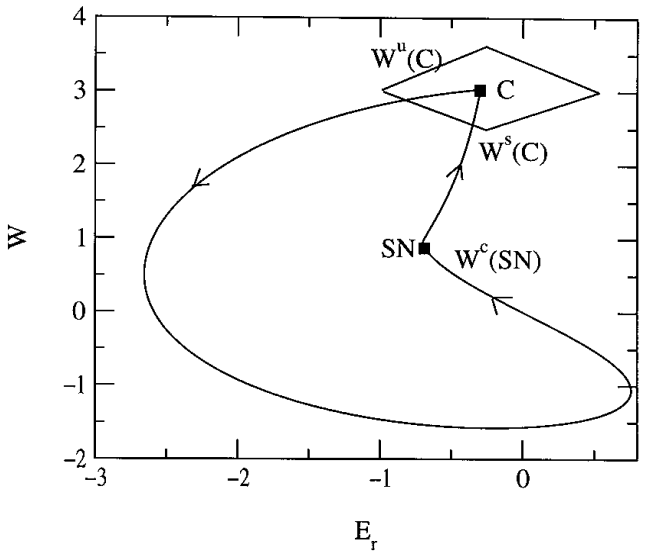

Fig. 18. T-point bifurcation: phase portrait of heteroclinic cycle between fixed point C and saddle-node fixed point (SN) at $(\beta, \eta) = (-1.117, 0.91595)$. The stable manifold $W^s(C)$ is one-dimensional while the unstable manifold $W^u(C)$ is two-dimensional. $W^c(SN)$ denotes the central manifold of the SN fixed point.

5. Conclusions and Outlooks

In this work a detailed study of the partial bifurcation set around the Type II regime of the Hopf-saddle-node singularity in a laser with an injected signal has been performed. Secondary Hopf bifurcations to a transversal and longitudinal (to the $W = 0$ plane) periodic orbit dominate the periodic motion in a region of parameter space where no locking solutions exists. The former periodic orbit is well described by the unfolding of the HSN bifurcation, and corresponds to undamped relaxation oscillations, while the latter arises as a saddle-node infinite-period (Andronov) global bifurcation. Our results show how the Arnold tongues arising from the transversal torus are "truncated" in parameter space by resonances of the longitudinal torus. Thus in phase space the periodic orbits are observed to deform continuously from transversal into longitudinal orbits. A partial bifurcation set displaying our main result is shown in Fig. 19.

Our work also extends [Solari & Oppo, 1994] results on the averaged LIS equations. The averaged system displays: (a) an Andronov bifurcation creating a longitudinal orbit, (b) a secondary longitudinal Hopf bifurcation on this orbit, which originates from the HSN point in parameter space, and (c) the characteristic transversal secondary Hopf bifurcation of the Type II HSN singularity. However, Solari and Oppo observed singular behavior (orbits going to infinity) as well when continuing the resulting tori in parameter space. The reason for this is the topological restriction to the deformation of transversal into longitudinal tori in a two-dimensional phase space.

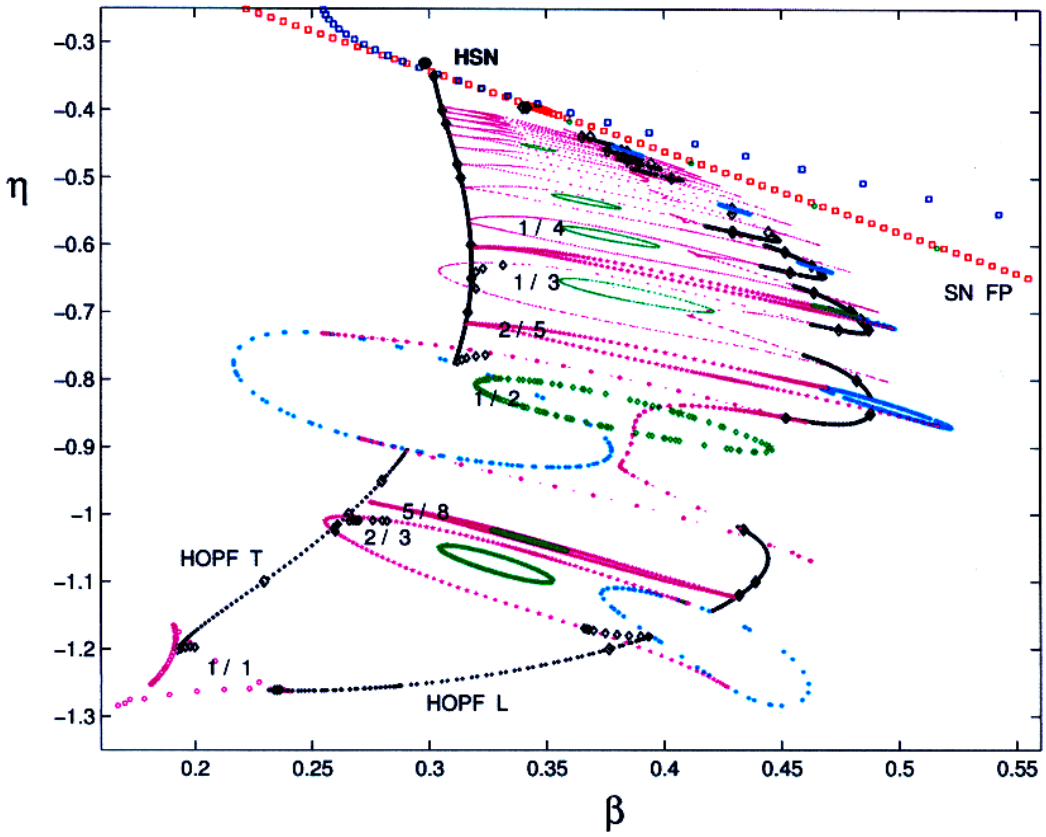

Fig. 19. Partial numerical bifurcation set for Type II HSN in LIS.

In the three-dimensional setting of LIS equations we have found instead a family of homoclinic orbits to the off-state fixed point, arranged in isolas in parameter space *inside each Arnold tongue* of the corresponding transversal torus. The off-state fixed point appears to be at infinity in the averaged equations (due to the change of coordinates), and hence we can conjecture that the singular behavior observed in the average model results from "bifurcations with infinity" [Sparrow & Swinnerton-Dyer, 1995], as we move between both tori. A more detailed study of the averaged equations would be desirable to test this conjecture.

Our present work is also related to a recent work on solid-state lasers with optical injection [Yeung & Strogatz, 1998], where a complicated bifurcation diagram close to the saddle-node bifurcation was found. The rate equations studied may be shown to be rescaled to LIS equations (1) with $\theta = 0$ (provided that $g \neq 0$). This particular detuning was shown by Solari and Oppo to be somewhat more delicate, but Type II HSN was preserved. Yeung and Strogatz studied the attractors in a parameter cut with constant detuning η, and increasing β approaching the saddle-node bifurcation. Their diagrams showed periodic windows, interspeded by orbits with a large intensity, reminiscent of the homoclinic orbit to the off-state found in our work. The most remarkable difference, is that the self-similar structure of periodic windows is reported to accumulate at the saddle-node of fixed points. Instead our work shows that (at least for $\theta = 0.5 > 0$), a *finite* number of resonances are crossed by constant-η cuts in the bifurcation diagram while approaching the saddle-node bifurcation. Nevertheless, it appears that the number of crossed resonances diverge as η approaches the codimension-2 value. Further work should confirm how the secondary Hopf bifurcation we found moves in parameter space as $\theta \to 0$.

Despite the complicated bifurcation set presented, we emphasize that most of this structure remains out of bound of standard experimental setups. Nevertheless we would like to point out that a partial confirmation of this bifurcation set should be possible, by following the stable *cw* solution in parameter space, and looking for stable undamped relaxation oscillations. The region of existence of

these two stable invariant sets is bounded by the secondary Hopf bifurcation, and by locating the locking region, this may validate the basic features of the Type II HSN scenario.

Finally, we would like to emphasize the possible implications of the homoclinic bifurcations to the laser off-state found above. Although this bifurcation was also observed in the previous analysis for Types of HSN, it appears that in the Type II regime this bifurcation has been singled out. The sequence of homoclinic bifurcations for each of the infinite number of resonances *accumulating* towards the HSN singularity is a remarkable result which needs further detailed study. This phenomenon suggests that the Hopf-saddle-node singularity may have, on top of the saddle-node infinite-period global bifurcation, another pair of heteroclinic orbits to the HSN fixed point, forming a cycle. So far, we are no longer surprised by the bizarre global bifurcations found in this laser, which provide stimulating motivation for further research.

Acknowledgments

It is a pleasure to thank Hernán Solari for helpful discussions. M. G. Zimmermann acknowledges a postdoc from FOMEC-UBA. C. Mayol acknowledges financial support from DGES (Spain) under Project Nos. PB94-1167 and PB97-0141-C02-01 and a MEC (Spain) fellowship.

References

Arnold, V. [1983] *Geometrical Methods in the Theory of Ordinary Differential Equations* (Springer-Verlag, NY).

Aronson, D. G., Chory, M. A., Hall, G. R. & McGehee, R. P. [1982] "Bifurcations from an invariant circle for two-parameter families of maps of the plane: A computer-assisted study," *Commun. Math. Phys.* **83**, 303–354.

Bykov, V. V. [1993] "The bifurcations of separatrix contours and chaos," *Physica* **D62**, 290–299.

Doedel, E., Fairgrieve, T., Sandstede, B., Champneys, A., Kuznetsov, Y. & Wang, S. [1997] *AUTO 97: Continuation and Bifurcation Software for Ordinary Differential Equations*, http://indy.cs.concordia.ca/auto/main.htm.

Glendinning, P. & Sparrow, C. [1986] "T-points: A codimension two heteroclinic bifurcation," *J. Stat. Phys.* **43**(3&4), 479–488.

Guckenheimer, J. & Holmes, P. J. [1983] *Nonlinear Oscillations, Dynamical Systems and Bifurcations of Vector Fields* (Springer Verlag, NY).

Hirschberg, P. & Laing, C. [1995] "Succesive homoclinic tangencies to a limit cycle," *Physica* **D89**, 1–14.

Kirk, V. [1991] "Breaking of symmetry in the saddle-node Hopf bifurcation," *Phys. Lett.* **A154**(5&6), 243–248.

Kuznetsov, Y. [1997] *Elements of Applied Bifurcation Theory*, Applied Mathematical Sciences Vol. 112 (Springer).

Oppo, G.-L., Politi, A., Lippi, G.-L. & Arecchi, F. T. [1986] "Frequency pushing in lasers with injected signal," *Phys. Rev.* **A34**, p. 4000.

Šil'nikov, L. P. [1965] "A case for the existance of a denumerable set of periodic motions," *Sov. Math. Dokl.* **6**, 163–166.

Šil'nikov, L. P. [1966] "On the generation of a periodic motion from a trajectory which leaves and re-enters a saddle-saddle state of equilibrium," *Sov. Math. Dokl.* **7**(5), 155–1158.

Simpson, T., Liu, J. M., Huang, K. F. & Tai, K. [1997] "Nonlinear dynamics induced by esternal optical injection in semiconductor lasers," *Quant. Semiclass. Opt.* **9**, 765–784.

Solari, H. G. & Oppo, G.-L. [1994] "Laser with injected signal: Perturbation of an invariant circle," *Opt. Commun.* **111**, 173–190.

Sparrow, C. & Swinnerton-Dyer, H. P. F. [1995] "The Falkner–Skan equation I: Creation of strange invariant sets," *J. Diff. Eqs.* **199**(2), 336–394.

Tredicce, J. R., T. F., Lippi, G.-L. & Puccioni, G. P. [1985] "Instabilities in lasers with an injected signal," *J. Opt. Soc. Am.* **B2**(1), p. 173.

van Tartwijk, G. H. M. & Lenstra, D. [1995] "Semiconductor lasers with optical injection and feedback," *Quant. Semiclass. Opt.* **7**, 87–143.

Wieczorek, S., Krauskopf, B. & Lenstra, D. [2000] "A unifying view of bifurcations in semiconductor lasers subject to optical injection," *Opt. Commun.* **172**, 279–295.

Wiggins, S. [1991] *Introduction to Applied Nonlinear Dynamical Systems and Chaos*, Text in Applied Mathematics, Vol. 2 (Springer-Verlag).

Yeung, M. K. S. & Strogatz, S. [1998] "Nonlinear dynamics of a solid-state laser with injection," *Phys. Rev.* **E58**, 4421–4435.

Zimmermann, M. G., Natiello, M. A. & Solari, H. G. [1997] "Šil'nikov-saddle-node interaction: Laser with injected signal," *Physica* **D109**(3&4), 293–314.

Zimmermann, M. G. & Natiello, M. A. [1998] "Homoclinic and heteroclinic bifurcations close to a twisted heteroclinic cycle," *Int. J. Bifurcation and Chaos* **8**(2), 359–375.

Zimmermann, M. G., Natiello, M. A. & Solari, H. G. [2001] "Global bifurcations in a laser with injected signal: Beyond Adlers approximation," *Chaos* **11**(3), 500–513.